

Primary recrystallization of a magnesium hybrid material fabricated by high-pressure torsion

Ouarda Ould Mohamed¹, Piotr Bazarnik², Yi Huang^{3,4}, Hiba Azzeddine^{1,*}, Thierry Baudin⁵, François Brisset⁵, Megumi Kawasaki⁶, Terence G. Langdon³

¹ Laboratory of Materials and Renewable Energy, Faculty of Sciences, Mohamed Boudiaf University, 28000 M'sila, Algeria

² Warsaw University of Technology, Faculty of Materials Science and Engineering, Woloska 141, 02-507, Poland

³ Materials Research Group, Department of Mechanical Engineering, University of Southampton, Southampton SO17 1BJ, UK

⁴ Department of Design and Engineering, Faculty of Science and Technology, Bournemouth University, Poole, Dorset BH12 5BB, UK

⁵ Université Paris-Saclay, CNRS, Institut de Chimie Moléculaire et des Matériaux d'Orsay, 91405 Orsay, France

⁶ School of Mechanical, Industrial and Manufacturing Engineering, Oregon State University, Corvallis, OR 97331, USA

* Corresponding author: Prof. Hiba Azzeddine, hiba.azzeddine@univ-msila.dz

Abstract

The static recrystallization and grain growth of a hybrid AZ31/Mg-0.6Gd (wt.%) material fabricated by high-pressure torsion (HPT) through 20 turns were explored after isochronal annealing at 150, 250, 350 and 450 °C for 1 h using electron backscatter diffraction, transmission electron microscopy and Vickers microhardness measurements. The results reveal heterogeneity in the grain size distributions of the AZ31 and Mg-0.6Gd regions after annealing at the lower temperatures of 150 and 250 °C leading to a clear AZ31/Mg-0.6Gd interfacial border. At the higher temperatures of 350 and 450 °C the AZ31/Mg-0.6Gd interfaces were not well-defined owing to the occurrence of grain growth. It is shown that grain growth is restricted in the AZ31 and Mg-0.6Gd regions due to the presence of stable nano-size Al₈Mn₅ particles and the precipitation of Mg₁₇Al₁₂ and Mg₁₂Zn at 250 °C and of Mg₅Gd and Mg₁₂Gd phases at 350 and 450 °C. The distribution of the basal texture in both regions was strongly controlled by dynamic recrystallization, precipitation and grain growth. The values of the microhardness over the radial cross-sections of the hybrid discs decrease and become more uniform, in the range of ~35–66 Hv, with increasing annealing temperature.

Keywords: High-pressure torsion; Hybrid metal; Magnesium; Precipitation; Recrystallization

1. Introduction

The fabrication of hybrid metals by solid-state bonding is an effective concept for creating a new generation of functional materials with exceptional mechanical and structural properties which meet industrial requirements [1]. These hybrid metals can be fabricated using different techniques such as mechanical alloying [2], friction stir processing [3] and severe plastic deformation (SPD) [4].

During the last decade, the use of the high-pressure torsion (HPT) technique became not only well established for achieving significant grain refinement but also became a powerful methods for synthesizing new hybrid metals [5, 6]. Moreover, HPT processing has the ability to change the deformation behaviour and the dynamic recrystallization kinetics of Mg-based alloys by comparison with conventional thermomechanical processing [7, 8].

Recently, a novel hybrid material was successfully fabricated from separate discs of dissimilar Mg-based alloys (AZ31 and Mg-Gd) using HPT processing at room temperature [9]. It was found that the grain refinement in the hybrid material occurs through two stages due to the strain induced by HPT processing and an additional strain from the formation of interface bonding [9]. Furthermore, the hybrid AZ31/Mg-0.6Gd material exhibited a different texture than the undesirable strong basal texture that is usually formed in conventionally deformed Mg-based alloys and causes subsequent poor formability. The hybrid AZ31/Mg-0.6Gd material has a strong chance of replacing the conventional AZ31 alloy often used as lightweight structural material in the transportation industries, as well as a possible biodegradable implant material in biomedical applications [10, 11].

Numerous investigations are now available exploring the properties of hybrid materials related to the bonding and grain refinement and the formation of intermetallic phases during post deformation [5, 6, 9, 12, 13]. However, less attention has been given to the effect of heating on the evolution of properties and the thermal stability of hybrid metals [14] and in practice post-deformation annealing treatments are necessary to release the stored energy into a recrystallized microstructure with optimized grain size and modified texture. Accordingly, the purpose of the present study was to fully characterize the microstructure and mechanical properties of an AZ31/Mg-0.6Gd (wt.%) hybrid material fabricated by HPT processing after an isochronal annealing treatment.

2. Experimental material and procedures

The details of the AZ31 and Mg-0.6Gd alloys and the HPT processing conditions were given earlier [9]. In brief, AZ31 and Mg-0.6Gd discs with diameters of 10 mm and thicknesses of 0.85 mm were placed on the lower and the top anvil of the HPT facility, respectively. Then these two discs were processed by HPT at room temperature for 20 HPT turns under a pressure of 6.0 GPa with a rotational speed of 1 rpm and using quasi-constrained conditions [9]. The HPT-processed discs were subjected to isochronal annealing in a radiation furnace at 150, 250, 350 and 450 °C for 1 h.

The microstructure, texture and Vickers microhardness (Hv) measurements were undertaken on the cross-sectional (CD-SD) planes of the annealed discs as illustrated in Figure 1 where the shear reference frame is defined as the shear direction (SD), rotational direction (RD) and compression direction (CD), respectively.

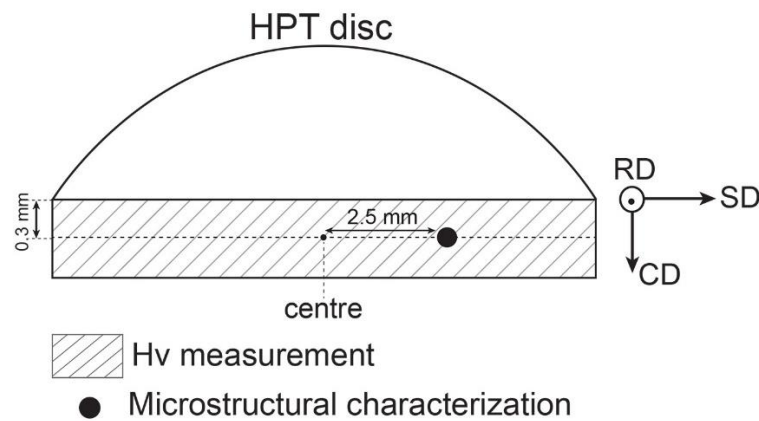


Figure 1: Schematic illustration showing the positions for the microstructure and microhardness measurements on the vertical cross-section of the HPT disc: SD, CD, and RD are the coordinate system.

Structural observations of the fabricated materials were collected using a scanning electron microscope (SEM) Hitachi Su8000 operating in back-scattered electron (BSE) mode. Observations were carried out on cross-sectional planes approximately 1 mm from the edges of the discs. Samples for the SEM investigations were prepared using a Hitachi IM4000 ion milling system. This procedure gives high-quality surfaces for observation due to ion beam polishing which eliminates any deformation, stresses and/or the formation of oxide layers. The surface quality after the ion milling permitted the structure to be observed in so-called channel contrast showing the grain boundaries in the material. These SEM observations were

complemented by electron back-scattered diffraction (EBSD) measurements performed near the mid-radius positions of the mid-thickness planes of the annealed discs (see Figure 1) using a TSL-EDAX-Hikari system mounted on a scanning electron microscope (FEG-SEM ZEISS Supra 55 VP) operating at 20 kV. The scanned areas for the discs annealed at 150 and 250 °C were $40 \times 40 \mu\text{m}^2$ with a 50 nm step size. The scanned area for the disc annealed at 350 °C was $100 \times 100 \mu\text{m}^2$ with a step size of 0.1 μm and the scanned area for the disc annealed at 450 °C was $200 \times 200 \mu\text{m}^2$ with a step size of 0.1 μm . The EBSD data were analysed by the Orientation Imaging Microscopy OIMTM software by considering a grain tolerance angle of 5° and a minimum grain size of 5 pixels.

The texture was analysed using MTEX software by calculating the orientation distribution function (ODF) using the harmonic method ($L = 22$) and a Gaussian function with a half-width of 5° to model each orientation [15].

Detailed microstructural observations of selected areas were performed using a CS-corrected dedicated scanning transmission electron (STEM) Thermo Fisher Scientific Spectra microscope operating at an accelerating voltage of 200 kV. The STEM observations were carried out in the bright-field (BF) and high-angle annular dark field (HAADF) modes. Structural investigations were combined with advanced energy dispersive X-Ray (EDX) point and mapping analyses. Thin foils for observations were prepared using a Focused Ion Beam (FIB) Hitachi NB-5000 microscope.

Color-coded contour Vickers microhardness maps were constructed over the cross-sections of the annealed discs (see Figure 1) by using a Mitutoyo HM-200 facility with a load of 50 gf and a dwell time of 10 s.

3. Experimental results

Figure 2 shows the inverse pole figure (RD-IPF) maps near the AZ31/Mg-0.6Gd interface of the discs annealed at (a) 150, (b) 250, (c) 350 and (d) 450 °C, respectively. The grain boundaries with high misorientations (HAGBs, $\theta > 15^\circ$) are highlighted by a black line. In addition, the AZ31 and Mg-0.6Gd regions are indicated in each map. It should be noted that the RD-IPF map of the disc annealed at 450 °C (Figure 2d) is shown with a different scale bar. Figure 3 displays the evolution of the mean grain size of the AZ31 and Mg-0.6Gd regions as a function of annealing temperature.

The microstructures are heterogeneous in the discs annealed at 150 and 250 °C where the AZ31 and Mg-0.6Gd regions are easily identified. The AZ31 region of the annealed disc at 150 °C, as shown in Figure 2a, is characterized by a black zone referring to the non-index area

which is a consequence of the large amounts of deformation. This may suggest that annealing at 150 °C for 1 h is not sufficient for the occurrence of static recrystallization of the AZ31 region. A net difference in the grain size distribution is apparent between the AZ31 and Mg-0.6Gd regions in the disc annealed at 250 °C, as shown in Figure 2b. Thus, the microstructure becomes more homogeneous in discs annealed at 350 and 450 °C in which the AZ31/Mg-0.6Gd interfaces are hardly recognized. Some coarse grains are visible in the Mg-0.6Gd region after annealing at 350 °C (Fig. 2(c)) and these grains are further coarsened at 450 °C. In addition, the white arrows in Figure 2d indicate the presence of annealing twins in the AZ31 and Mg-0.6Gd regions of the disc annealed at 450 °C. The formation of annealing twins is often observed in various annealed Mg-based alloys [16-19]. The mean grain size evolution shown in Figure 3 demonstrates that the mean grain size of the Mg-0.6Gd region continuously increases from $0.8 \pm 0.2 \mu\text{m}$ at 150 °C to a value of $6.5 \pm 0.8 \mu\text{m}$ at 450 °C.

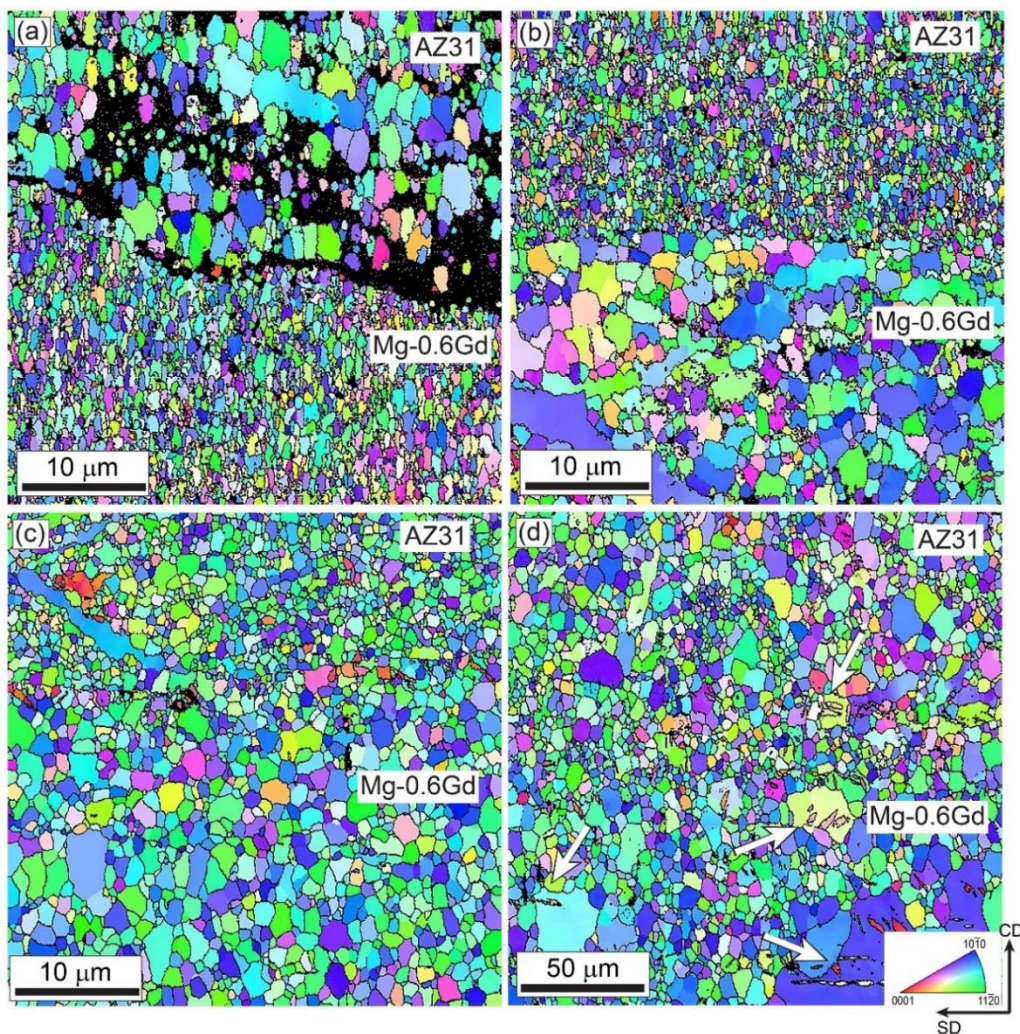


Figure 2: RD-IPF maps near the AZ31/Mg-0.6Gd interfaces of the hybrid material after isochronal annealing for 1 h at: (a) 150, (b) 250, (c) 350, and (d) 450 °C.

For the record, it should be noted that the grain sizes of the AZ31 and Mg-0.6Gd regions after HPT processing for 20 turns was reported earlier as 0.1 and 0.4 μm , respectively [9]. The mean grain size of the AZ31 region also increases with increasing annealing temperature except that the mean grain size is lower at 250 $^{\circ}\text{C}$ (0.6 \pm 0.3 μm) than at 150 $^{\circ}\text{C}$ (1.7 \pm 0.5 μm). The AZ31 region exhibits a smaller grain size than the Mg-0.6Gd region through the annealing temperature range of 250–450 $^{\circ}\text{C}$.

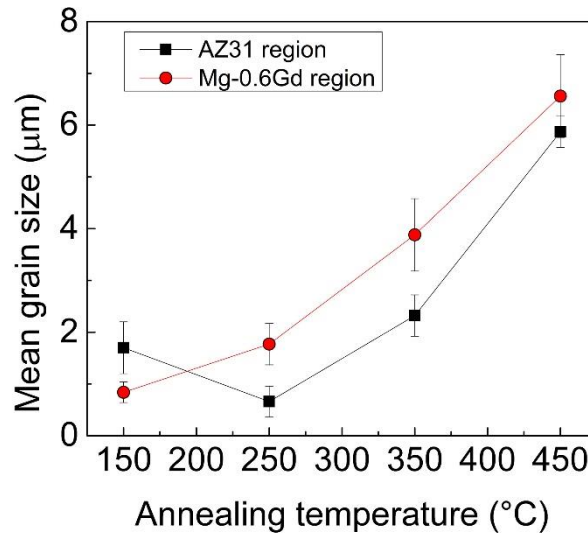


Figure 3: Evolution of the mean grain size of the AZ31 and Mg-0.6Gd regions as a function of annealing temperature.

Figure 4 displays histograms of the grain boundary misorientation distributions for the AZ31 and Mg-0.6Gd regions as a function of annealing temperature. The grain boundary misorientation distribution for randomly oriented material with an hexagonal structure is added for comparison [20]. In addition, the fraction of HAGBs in each region is also shown in the plots. It is apparent that the AZ31 and Mg-0.6Gd regions do not show any random distribution under the isochronal annealing. Indeed, the grain boundary distribution shows a peak around 30 $^{\circ}$ indicating a 30 $^{\circ}$ $\langle 0001 \rangle$ grain boundary resulting from the formation of a basal texture [21]. This peak tends to disappear in the AZ31 and Mg-0.6Gd regions annealed at 350 and 450 $^{\circ}\text{C}$, respectively. Figure 3d shows a peak around 86 $^{\circ}$ for both regions indicating the presence of an extension twin (86 $^{\circ}$ $\langle 11-20 \rangle$). The fraction of HAGBs increases with increasing annealing temperature in both AZ31 and Mg-0.6Gd regions due to the formation of recrystallized grains.

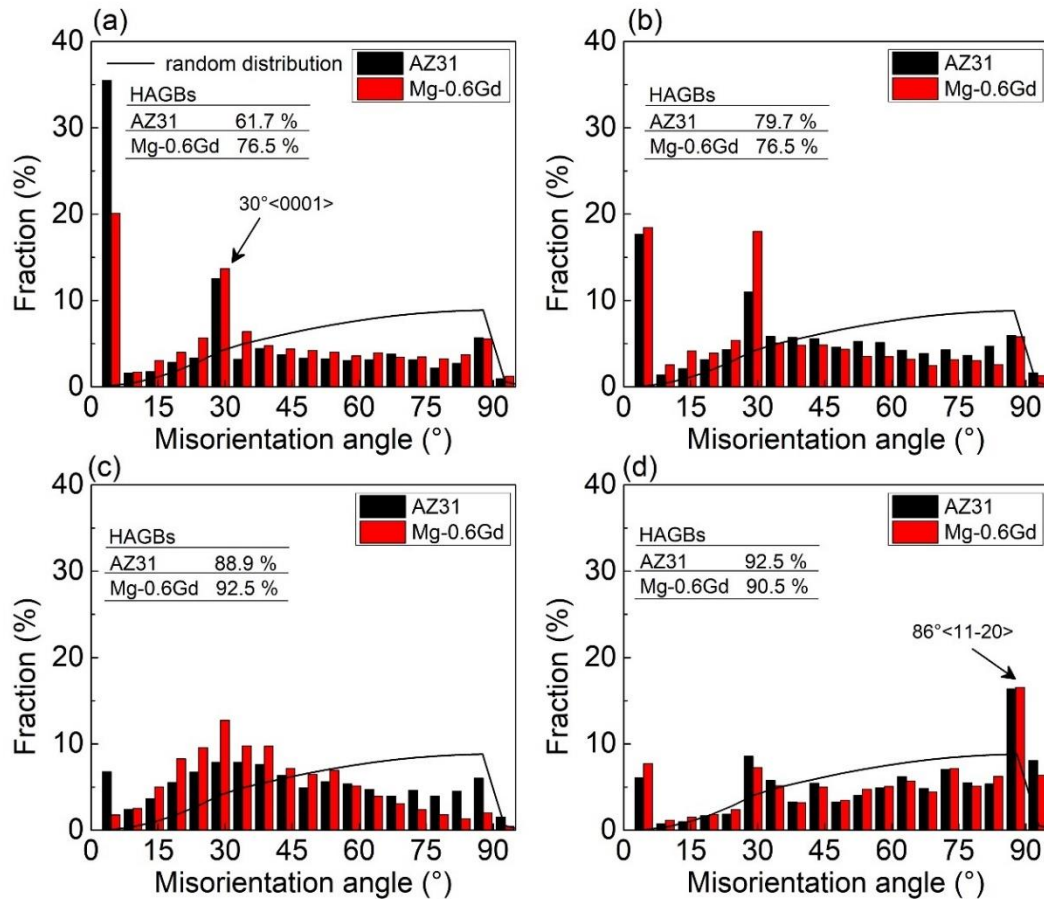


Figure 4: Histograms of the grain boundary misorientation distributions in the AZ31 and Mg-0.6Gd regions as a function of annealing temperature: (a) 150, (b) 250, (c) 350 and (d) 450 °C.

The SEM micrographs with different magnifications near the AZ31/Mg-0.6Gd interfaces of the isochronal annealed discs are presented in Figure 5. It was found that the AZ31 region under the HPT processing condition contained nano-sized Al_8Mn_5 (~10-45 nm) and nano-sized $Mg_{17}Al_{12}$ (~10-24 nm) particles [8, 9]. Moreover, the HPT processing caused the fragmentation of the Mg_5Gd phase initially present in the as-cast condition of the Mg-0.6Gd region [8, 9]. The SEM micrograph of the disc annealed at 150 °C (Figure 5a) shows an equiaxed microstructure of the hybrid material except that the mean grain size of the Mg-0.6Gd region is obviously smaller than for the AZ31 region which is in accordance with the EBSD measurements (Figures 2a and 3). Figure 5b indicates that there is a large number of precipitates in the AZ31 region at an annealing temperature of 250 °C whereas these precipitations are absent in the AZ31 regions in the discs annealed at 350 and 450 °C as shown in Figures 5c and 5d. The precipitation occurs also in the Mg-0.6Gd region during annealing at 350 and 450 °C as observed in Figures 5c and 5d. However, the precipitation in the Mg-0.6Gd region at a

temperature of 450 °C tends to be less pronounced than in the Mg-0.6Gd region at a temperature of 350 °C thereby indicating the dissolution of precipitates.

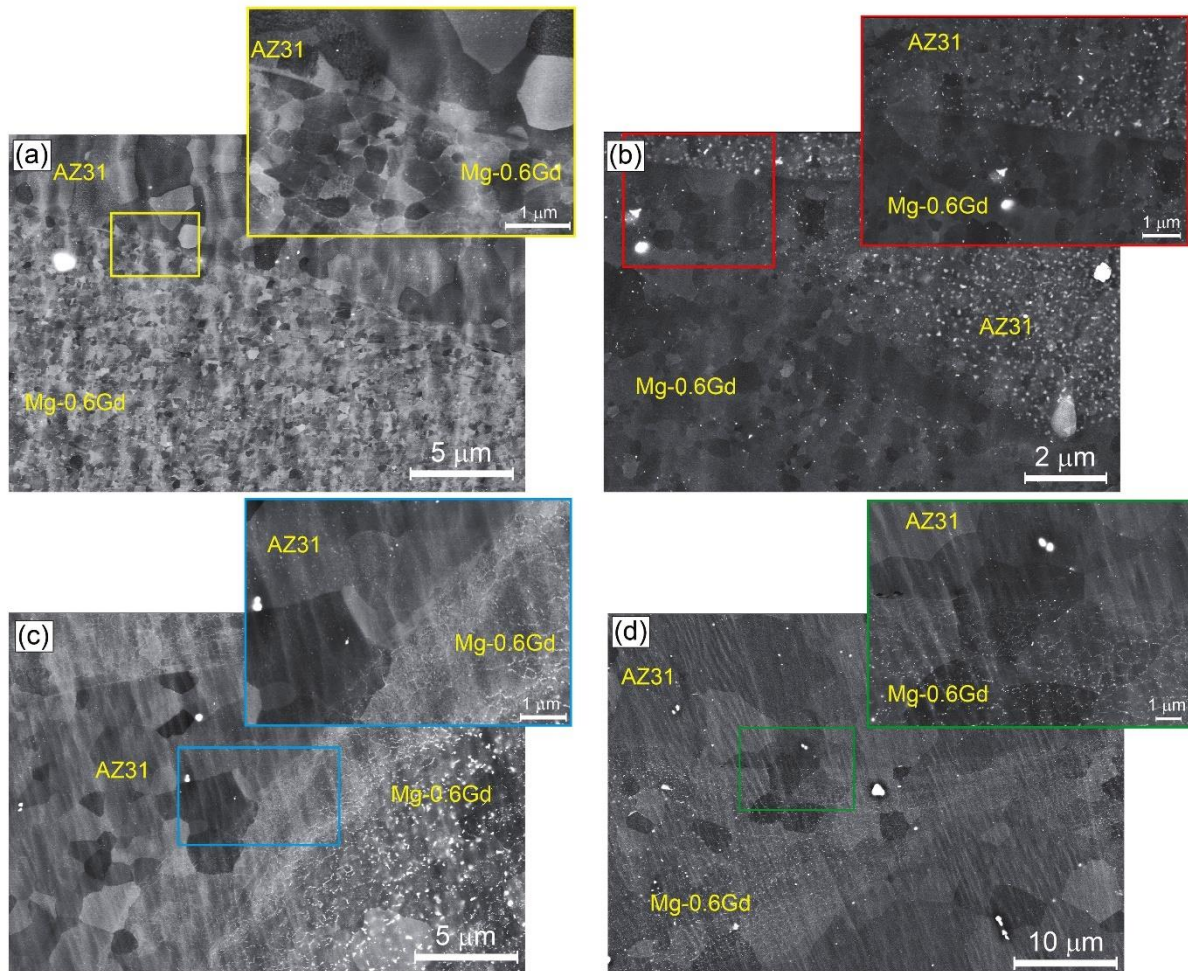


Figure 5: SEM micrographs with different magnifications near the AZ31/Mg-0.6Gd interfaces after annealing for 1 h at: (a) 150, (b) 250, (c) 350, and (d) 450 °C.

HAADF-STEM and EDS mapping for the Mg, Al, Zn, Mn and Gd elements shown in Figure 6 was used to identify the precipitates observed in the annealed AZ31 region at 250 °C and the annealed Mg-0.6Gd region at 350 °C, respectively. The EDS analysis of different particles (points 1–5) is summarized in the Table shown also in Figure 6. The annealed AZ31 region at 250 °C contains three types of second phases with different chemical compositions. First, nano-sized particles of Al_8Mn_5 (point 1) with a size of 10 nm are distributed homogeneously in the entire AZ31 region. Second, large $\text{Mg}_{17}\text{Al}_{12}$ precipitates (point 2) with lengths of 50-90 nm are localized preferably along grain boundaries in the region and, in addition, spherical $\text{Mg}_{17}\text{Al}_{12}$ particles with diameters of ~10-40 nm are homogeneously distributed in the AZ31 region which are similar to those reported under the deformation

condition [9]. Third, particles with a diameter of 40 nm are present within the grains containing only Mg and Zn elements as indicated by point 3 which was identified as the $Mg_{12}Zn$ phase. A close examination of Zn element mapping of the AZ31 region annealed at 250 °C indicates the segregation of Zn elements at the grain boundaries. By contrast, the Mg-0.6Gd region annealed at 350 °C shows the presence of two types of second-phase particles, corresponding to precipitation of an Mg_5Gd phase (point 4) at the grain boundaries and nano-sized particles of $Mg_{12}Gd$ (point 5) with a diameter of 17 nm distributed reasonably homogeneously within the microstructure.

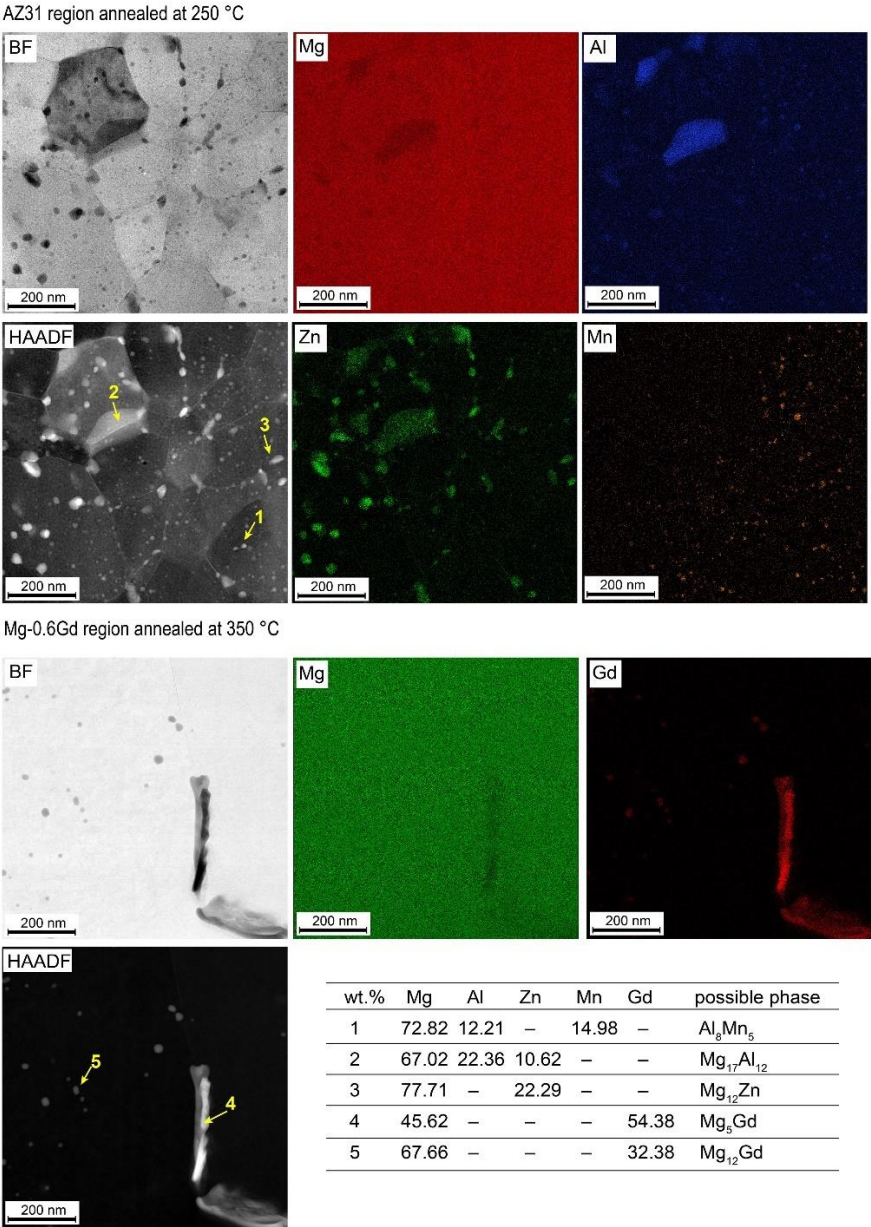


Figure 6: STEM images in BF and HAADF modes and EDS mapping for Mg, Al, Zn, Mn and Gd elements and EDS analysis of particles present at points 1–5 of the AZ31 region annealed at 250 °C and the Mg-0.6Gd region annealed at 350 °C.

Figure 7 presents the recalculated $\{0002\}$ pole figures, from left, near the AZ31/Mg-0.6Gd interface of the hybrid material, AZ31, and Mg-0.6Gd regions after annealing at (a) 150, (b) 250, (c) 350 and (d) 450 °C, respectively. It is noted that the texture near the mid-radius of the hybrid disc processed for 20 turns was characterized by a deviated basal texture [9]. As is apparent from Figure 7, a typical basal texture developed in the hybrid material during annealing at 150 through 350 °C and a net scattering of the basal pole from CD towards SD is visible for the hybrid disc annealed at 450 °C. It was reported earlier that the AZ31 region of the hybrid material fabricated by HPT at 20 turns developed a C_2 -fiber with a weak C_1 -fiber texture, while a deviated basal texture was formed in the Mg-0.6Gd region [9]. The texture evolutions of the AZ31 and Mg-0.6Gd regions are quite similar as a function of annealing temperature. In practice, both regions exhibit a basal texture where the basal $\{0002\}$ planes of the grains are preferentially oriented parallel to the shear (SD-RD) plane but their distribution around CD changed during annealing at different temperatures. The scattering of the basal pole at an annealing temperature of 450 °C is more pronounced in the AZ31 region. By contrast, the texture of the Mg-0.6Gd region exhibits a spread of the basal texture from CD towards SD with a high intensity around the orientation of (180°, 35°, 0°) as indicated by arrows in Figure 7d.

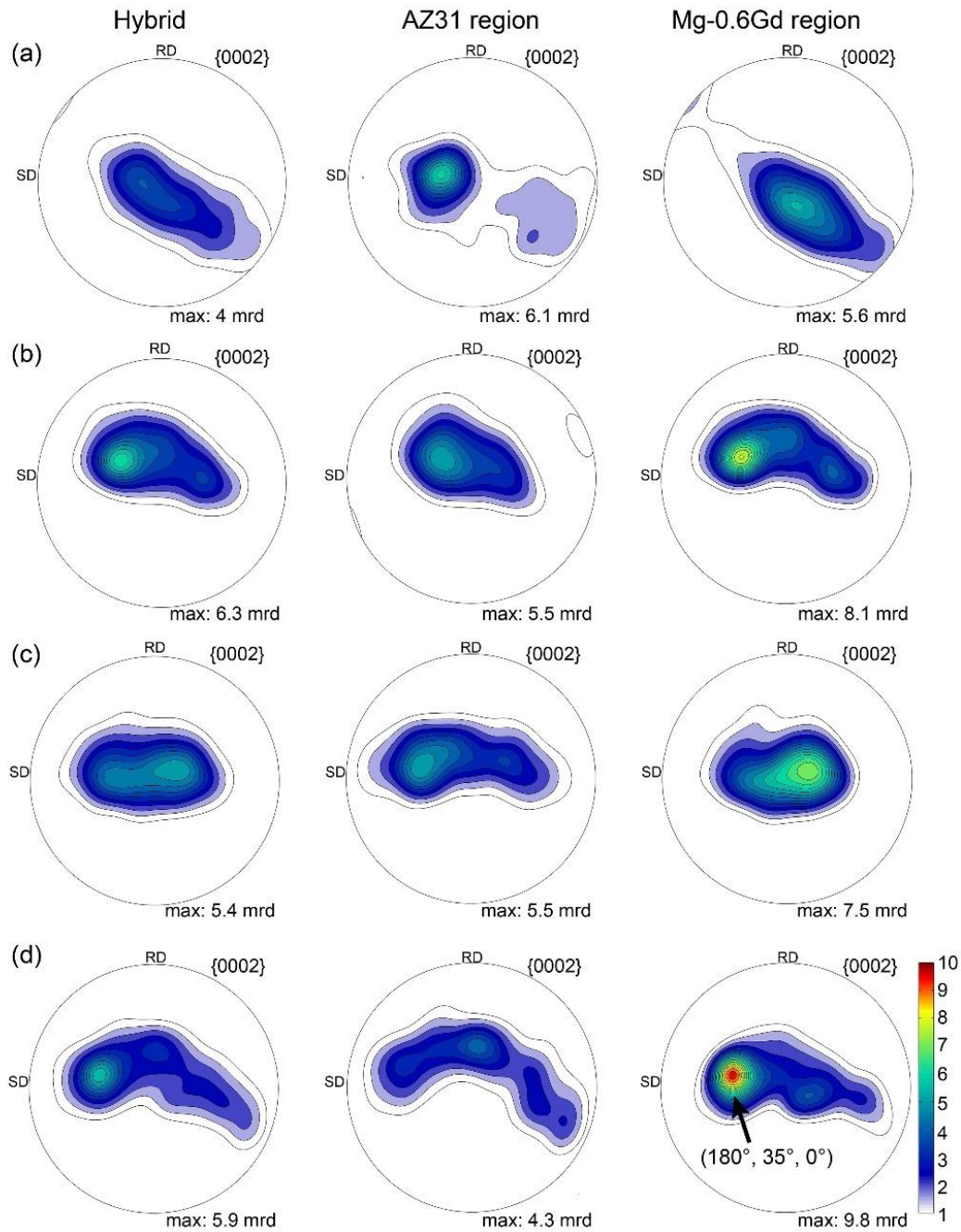


Figure 7: Recalculated $\{0002\}$ pole figures of the hybrid AZ31/Mg-0.6Gd material, the AZ31 and the Mg-0.6Gd regions after annealing at: (a) 150, (b) 250, (c) 350, and (d) 450 °C.

Figure 8 presents microhardness maps taken over the cross-sections of the hybrid AZ31/Mg-0.6Gd material after isochronal annealing. Usually, the Vickers microhardness values of the deformed and recrystallized AZ31 alloy are in the range of 60-120 Hv [8, 9, 22, 23]. In the case of Mg-0.6Gd alloy, the Vickers microhardness value was found in the range of 24-53 Hv [8, 9]. Consequently, it appears that the AZ31 and Mg-0.6Gd regions are in the upper and lower parts of the discs, respectively. The highest microhardness values in the range of

98– 130 Hv are located in the upper periphery of the disc annealed at 150 °C (Figure 8a). Then the microhardness values decrease with increasing annealing temperature due to recrystallization and grain growth. In addition, the microhardness variations became less across the AZ31 and Mg-0.6Gd regions when annealing at higher temperatures. For example, microhardness values were recorded in the range of 35–66 Hv after annealing at 450 °C (see Figure 8d).

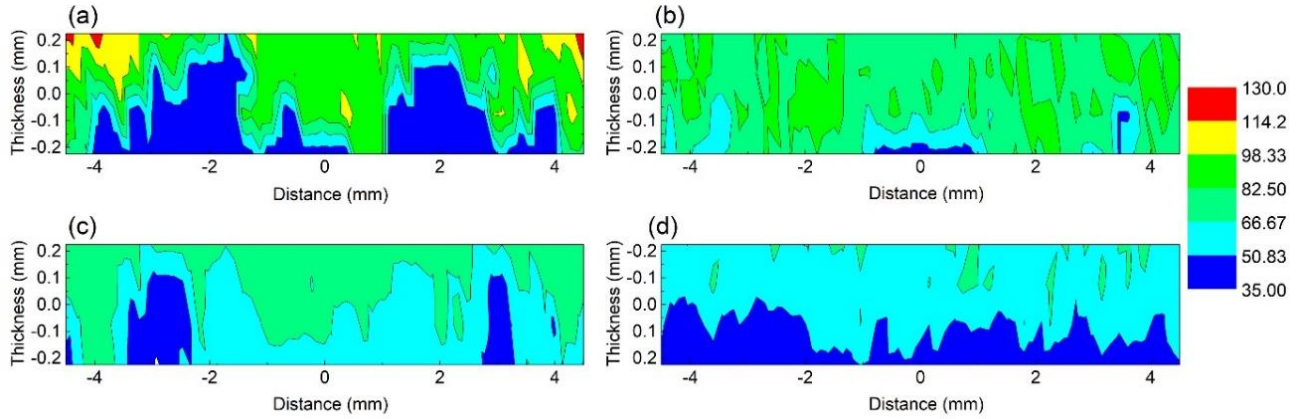


Figure 8: Color-coded microhardness maps of the hybrid AZ31/Mg-0.6Gd material after annealing for 1 h at: (a) 150, (b) 250, (c) 350, and (d) 450 °C.

The inhomogeneity factor (IF) [24] was used to evaluate the microstructural inhomogeneity of the hybrid discs as a function of annealing temperature and the estimated IF values are presented in Table 1. The equation for computing IF is given by:

$$IF = \frac{\sqrt{\sum_{i=1}^n (Hv_i - Hv_{ave})^2 / n - 1}}{Hv_{ave}} \times 100 \quad (1)$$

where Hv_{ave} and Hv_i are the average microhardness value and the microhardness value of the i^{th} measurement, respectively, and n is the number of microhardness measurements on each disc.

Table 1. IF values as a function of annealing temperature.

Temperature (°C)	150	250	350	450
IF (%)	36.3	13.8	17.4	16.9

Thus, a microstructure with less variation in the microhardness values exhibits a low IF value [24] and hence the discs annealed at 150 and 250 °C exhibit the highest (36.3%) and the lowest IF (13.8%) values, respectively. The IF value increases slightly to 17% during annealing at 350 and 450 °C indicating a minor increase in hardness variations across the regions.

4. Discussion

The present results demonstrate that the microstructure near the interfaces and the microhardness distributions through the disc surfaces become homogeneous over the vertical cross-sections of the hybrid AZ31/Mg-0.6Gd material after HPT followed by annealing with increasing annealing temperature. Nevertheless, the evolution of grain size and texture as a function of annealing temperature is slightly different between the AZ31 and Mg-0.6Gd regions and these separate regions, which form the hybrid alloy, undergo different static recrystallization and grain growth behaviors.

4.1. Microstructure evolution in the annealed AZ31 and Mg-0.6Gd regions

The distinctive outcome from the present investigation is the observation and identification of a large number of precipitates of $Mg_{17}Al_{12}$ and $Mg_{12}Zn$ in the AZ31 region at an annealing temperature of 250 °C and Mg_5Gd and $Mg_{12}Gd$ in the Mg-0.6Gd region at annealing temperatures of 350 and 450 °C. It is well known that the $Mg_{17}Al_{12}$ compound is the only precipitate phase that can develop in Mg-Al alloy even with low Al content such as the AZ31 alloy [25, 26]. However, precipitation of the $Mg_{12}Zn$ phase was not reported earlier in the AZ31 alloys under other thermomechanical processing. For the Mg-0.6Gd region, the precipitate phases were not expected after annealing since the alloy contained a very low Gd content (0.6%). According to the Mg-Gd binary phase diagram [27], the precipitation of the Mg_5Gd phase dissolves in the temperature range of 200–500 °C when the Gd content is <0.6 wt.%. Thus, the precipitation sequence in Mg-Gd alloy is usually investigated with Gd concentrations in the range of 10-15 Gd wt.% [28-31] and Mg alloys containing Gd concentrations around 1% are investigated in order to avoid the effect of second particles [32, 33].

It is known that HPT processing enhances precipitation due to the introduction of a large number of defects, such as dislocations and vacancies, that are preferential sites for precipitate nucleation [34]. However, it is noted that no precipitation was reported in the same Mg-0.6Gd alloy processed by HPT through 5 turns and annealed at 450 °C for 1h [35]. This led to the conclusion that the strain induced by HPT processing was not sufficient to produce non-equilibrium phases such as Mg_5Gd , $Mg_{12}Gd$ and $Mg_{12}Zn$. In addition to the high strain induced by HPT processing, it was demonstrated that the formation of interface bonding in the HPT-hybrid material by solid diffusion also induced strain that caused a second grain refinement regime [9]. Based on these earlier results, it may be anticipated that not only the accumulation of the high strain for grain refinement during HPT processing but also the formation of bonding of different phases produces a high number of defects, such as vacancies, and this produces an

unbalanced segregation of solute atoms and dislocations which act as preferential sites for precipitation nucleation during the annealing treatment. Usually, the precipitation causes an age hardening which could be detected by an increase in the microhardness values. However, it is considered that the $Mg_{17}Al_{12}$ compound plays only a minor role in the strengthening of the AZ31 alloy during conventional deformation due to its low volume fraction [25]. Unfortunately, it was not possible to confirm whether the precipitation of non-equilibrium Mg_5Gd , $Mg_{12}Gd$ and $Mg_{12}Zn$ phases caused an age hardening using the Hv map shown in Figure 8 since the AZ31 and Mg-0.6Gd regions were not easily identified and their Hv values could not be separated. Nevertheless, Table 1 shows that the IF of the microhardness distribution increases after annealing at 350 and 450 °C which may be explained by the strengthening of the Mg-0.6Gd region due to precipitation of the Mg_5Gd and $Mg_{12}Gd$ phases.

Precipitation in the AZ31 and Mg-0.6Gd regions plays the main role in controlling the evolution of grain size in both regions and throughout the hybrid material as well. The restricted grain growth noticed at the annealing temperature of 250 °C for the AZ31 region by comparison with the AZ31 region annealed at 150 °C (see Figure 3) which is mainly attributed to the precipitation of $Mg_{17}Al_{12}$ and $Mg_{12}Zn$ phases. Also, the segregation of Zn element to the grain boundaries as shown in Figure 6 produces a strong drag effect on grain boundary migration. It is believed that the presence of stable $Mg_{17}Al_{12}$ and Al_8Mn_5 phases are responsible for the small grain size during annealing temperatures superior to 250 °C. As shown in Figure 6, the majority of the precipitates and the stable phases are nano-sized which prevents the migration of recrystallized grain boundaries and thereby slows the grain growth rate of the recrystallized grains.

A further factor which produces a slow grain growth in the AZ31 region compared with the Mg-0.6Gd region (Figure 3) is the high content of solute elements in the AZ31 alloy (3% of Al and 1% of Zn). This leads to a significant reduction in the stacking fault energy through the solute–dislocation interaction and produces smaller grain sizes under HPT processing and annealing treatments. Indeed, it was demonstrated that the mean grain size decreases with decreasing stacking fault energy in the deformed material [36].

The presence of Mg_5Gd and $Mg_{12}Gd$ precipitates along the grain boundaries and within the recrystallized grains (Figure 6) suggests that the precipitation takes place after the static recrystallization. Hence, it is anticipated that the driving force of recrystallization is the stored energy during HPT which plays a major role in the Mg-0.6Gd region where the grain boundaries are only partially pinned by the precipitates. The mean grain size of the Mg-0.6Gd region increases with increasing annealing temperature even with the precipitation of Mg_5Gd and

Mg₁₂Gd phases at annealing temperatures of 350 and 450 °C but the mean grain size values remain much smaller (6.5 μm) than those reported for the same alloy under similar HPT processing and annealing conditions without precipitation (~20.1 μm) [35]. It is interesting to note that the AZ31 and Mg-0.6Gd regions have mean gain sizes smaller than 10 μm which suggests the hybrid material is a good candidate for achieving superplasticity [23].

4.2. Texture evolution in the annealed AZ31 and Mg-0.6Gd regions

The AZ31 and Mg-Gd alloys exhibit a retained deformation texture during recrystallization and grain growth phenomena [22, 35, 37, 38]. The present results show that the recrystallization textures of the AZ31 and Mg-0.6Gd regions are different from the deformation texture [9] and also they can be modified with appropriate annealing treatments.

The development of texture in the AZ31 and Mg-0.6Gd regions during isochronal annealing is a consequence of the contributions of dynamic recrystallization (DRX) [19, 38-40], precipitation [19, 35] and grain growth [41-43]. It was found earlier that the DRX fractions of the AZ31 and Mg-0.6Gd regions near the mid-radii of the hybrid discs processed for 20 HPT turns were 55 and 80 %, respectively [9]. This explained the change of the deformation texture from C₁ and C₂ fibres to a deviated basal texture at 150 °C in the case of the AZ31 region while the Mg-0.6Gd region annealed at 150 °C displays a retained deformation texture or deviated basal texture.

In the present study, the precipitation and grain growth in the AZ31 and Mg-0.6Gd regions occurred simultaneously and this made it difficult to separately evaluate their contributions to the texture evolution. Nevertheless, it is believed that the precipitated phases (Mg₁₇Al₁₂, Mg₁₂Zn, Mg₅Gd and Mg₁₂Gd) are the main reasons for the formation of a typical basal texture in the AZ31 region at 250 °C and in the Mg-0.6Gd region at 350 °C (Figures 7b and 7c), respectively. The precipitates drag the mobility of different grain boundaries except those of grains with a basal orientation that can preferentially grow during the annealing treatment and this leads to the domination of a basal texture. Indeed, the domination of the basal texture during an annealing treatment was attributed earlier to the high mobility of the grain boundaries of grains with a basal orientation [44]. Thus, the basal texture became more spread along SD with increasing annealing temperature for the AZ31 region, especially at 450 °C, due to the absence of second phase particles and the occurrence of grain growth that allowed the formation of recrystallized grains with different orientations. Annealing at high temperatures such as 450 °C provides the necessary energy for migration of the random high-angle grain boundaries, leading to uniform growth of recrystallized grains with different orientations rather

than the basal orientation. In addition, the fraction of sub-grain boundaries decreases significantly during high annealing temperatures, as shown in Figure 4(d). The sub-grain boundaries have low mobility energy and hence high temperature such as 450 °C gives these boundaries the opportunity to gradually transform into high-angle grain boundaries and form new grains. This process is known as continuous static recrystallization with the formed grains usually exhibiting different orientations [45]. The spread of basal texture for the Mg-0.6Gd region at 450 °C is less intense than in the AZ31 region due to the concurrent effects of precipitation and grain growth.

The present findings provide a clear demonstration that the application of various annealing temperatures produces unique microstructural pathways for these hybrid Mg alloys from well-defined phase boundaries to homogeneous microstructures with texture modifications. Thus, this study provides a critical initiative for using thermal treatments in the design and manufacture of Mg alloys and hybrids for different applications and opportunities.

5. Summary and conclusions

The evolution of microstructure, texture and Vickers microhardness in a hybrid AZ31/Mg-0.6Gd material fabricated by HPT through 20 turns was successfully characterized after isochronal annealing at 150, 250, 350 and 450 °C for 1 h. The main findings are as follows:

- The AZ31/Mg-0.6Gd interface disappeared during annealing temperatures higher than 350 °C where significant grain growth took place. In addition, the distributions of microhardness through the cross-sections of the discs became more homogeneous.
- The strain induced by HPT processing and interface bonding enhanced solute diffusion and caused the development of precipitation in the AZ31 and Mg-0.6Gd regions.
- Nano-sized stable particles of Al_8Mn_5 and precipitation of $Mg_{17}Al_{12}$ and $Mg_{12}Zn$ in the AZ31 region and precipitations of Mg_5Gd and $Mg_{12}Gd$ phases in the Mg-0.6Gd region contribute to a slowing in grain growth in the hybrid material.
- The distributions of basal texture in the AZ31 and Mg-0.6Gd regions throughout the annealing treatment of both regions was controlled by DRX, precipitation and grain growth.

Acknowledgements

Dr-Ing. N. Hort and Dr. D. Letzig (MagIC, Germany) and Dr-Ing. Talal Al-Samman (RWTH-Aachen University, Germany) are gratefully acknowledged for providing the AZ31 and Mg-

0.6Gd alloys, respectively. YH and TGL were supported by the European Research Council under Grant Agreement No. 267464-SPDMETALS. MK was supported by the National Science Foundation of the United States under Grant No. CMMI-2051205.

References

- [1] V. Rana, H. Kumar, A. Kumar, Fabrication of hybrid metal matrix composites (HMMCs) – A review of comprehensive research studies, *Materials Today: Proceedings* 56 (2022) 3102-3107.
- [2] C. Suryanarayana, Mechanical alloying: a critical review, *Materials Research Letters* 10(10) (2022) 619-647.
- [3] R.S. Mishra, Z.Y. Ma, I. Charit, Friction stir processing: a novel technique for fabrication of surface composite, *Materials Science and Engineering: A* 341(1) (2003) 307-310.
- [4] M. Kawasaki, J.-K. Han, D.-H. Lee, J.-i. Jang, T.G. Langdon, Fabrication of nanocomposites through diffusion bonding under high-pressure torsion, *Journal of Materials Research* 33(18) (2018) 2700-2710.
- [5] J.-K. Han, T. Herndon, J.-i. Jang, T.G. Langdon, M. Kawasaki, Synthesis of Hybrid Nanocrystalline Alloys by Mechanical Bonding through High-Pressure Torsion, *Advanced Engineering Materials* 22(4) (2020) 1901289.
- [6] D. Hernández-Escobar, M. Kawasaki, C.J. Boehlert, Metal hybrids processed by high-pressure torsion: synthesis, microstructure, mechanical properties and developing trends, *International Materials Reviews* 67(3) (2022) 231-265.
- [7] N. Stanford, M.D. Callaghan, B. de Jong, The effect of rare earth elements on the behaviour of magnesium-based alloys: Part 1—Hot deformation behaviour, *Materials Science and Engineering: A* 565 (2013) 459-468.
- [8] O. Ould Mohamed, P. Bazarnik, Y. Huang, H. Azzeddine, T. Baudin, F. Brisset, T.G. Langdon, A Comparative Study Between AZ31 and Mg-Gd Alloys After High-Pressure Torsion, *Journal of Materials Engineering and Performance* (2023).
- [9] O. Ould Mohamed, H. Azzeddine, Y. Huang, T. Baudin, P. Bazarnik, F. Brisset, M. Kawasaki, T.G. Langdon, Investigation of Microstructure and Texture Evolution in an AZ31/Mg-Gd Alloy Hybrid Metal Fabricated by High-Pressure Torsion, *Advanced Engineering Materials* 25(11) (2023) 2201794.
- [10] J. Song, J. She, D. Chen, F. Pan, Latest research advances on magnesium and magnesium alloys worldwide, *Journal of Magnesium and Alloys* 8(1) (2020) 1-41.
- [11] M.P. Medeiros, D.R. Lopes, M. Kawasaki, T.G. Langdon, R.B. Figueiredo, An Overview on the Effect of Severe Plastic Deformation on the Performance of Magnesium for Biomedical Applications, *Materials* 16(6) (2023) 2401.
- [12] P. Bazarnik, A. Bartkowska, Y. Huang, K. Szlązak, B. Adamczyk-Cieślak, J. Sort, M. Lewandowska, T.G. Langdon, Fabrication of hybrid nanocrystalline Al-Ti alloys by mechanical bonding through high-pressure torsion, *Materials Science and Engineering: A* 833 (2022) 142549.
- [13] S.O. Rogachev, R.V. Sundeev, V.M. Khatkevich, Evolution of the structure and strength of steel/vanadium alloy/steel hybrid material during severe plastic deformation, *Materials Letters* 173 (2016) 123-126.
- [14] D. Hernández-Escobar, R.R. Unocic, M. Kawasaki, C.J. Boehlert, High-pressure torsion processing of Zn-3Mg alloy and its hybrid counterpart: A comparative study, *Journal of Alloys and Compounds* 831 (2020) 154891.
- [15] R. Hielscher, H. Schaeben, A novel pole figure inversion method: specification of the MTEX algorithm, *Journal of Applied Crystallography* 41(6) (2008) 1024-1037.

- [16] J. Stráská, M. Janeček, J. Čížek, J. Stráský, B. Hadzima, Microstructure stability of ultra-fine grained magnesium alloy AZ31 processed by extrusion and equal-channel angular pressing (EX–ECAP), *Materials Characterization* 94 (2014) 69-79.
- [17] R.L. Doiphode, S.V.S.N. Murty, N. Prabhu, B.P. Kashyap, Grain growth in calibre rolled Mg–3Al–1Zn alloy and its effect on hardness, *Journal of Magnesium and Alloys* 3(4) (2015) 322-329.
- [18] M. Roostaei, M. Shirdel, M.H. Parsa, R. Mahmudi, H. Mirzadeh, Microstructural evolution and grain growth kinetics of GZ31 magnesium alloy, *Materials Characterization* 118 (2016) 584-592.
- [19] S. Tighiouaret, R. Lachhab, A. Hanna, H. Azzeddine, Y. Huang, T. Baudin, A.-L. Helbert, F. Brisset, D. Bradai, T.G. Langdon, Thermal Stability of an Mg–Nd Alloy Processed by High-Pressure Torsion, *Advanced Engineering Materials* 21(12) (2019) 1900801.
- [20] A. Morawiec, Misorientation-Angle Distribution of Randomly Oriented Symmetric Objects, *Journal of Applied Crystallography* 28(3) (1995) 289-293.
- [21] J.A. del Valle, M.T. Pérez-Prado, O.A. Ruano, The distribution of disorientation angles in a rolled AZ31 Mg alloy, *Revista de Metalurgia* 38(5) (2002) 353-357.
- [22] S. Sadi, A. Hanna, T. Baudin, A.-L. Helbert, F. Brisset, D. Bradai, H. Azzeddine, Evaluation of static recrystallization and grain growth kinetics of hot-rolled AZ31 alloy, *Journal of Metals, Materials and Minerals* 32(1) (2022) 12-26.
- [23] L.R.C. Malheiros, R.B. Figueiredo, T.G. Langdon, Grain size and microhardness evolution during annealing of a magnesium alloy processed by high-pressure torsion, *Journal of Materials Research and Technology* 4(1) (2015) 14-17.
- [24] S. Sadi, A. Hanna, H. Azzeddine, C. Casas, T. Baudin, A.-L. Helbert, F. Brisset, J.M. Cabrera, Characterization of microstructure and texture of binary Mg–Ce alloy processed by equal channel angular pressing, *Materials Characterization* 181 (2021) 111454.
- [25] X. Li, F. Jiao, T. Al-Samman, S. Ghosh Chowdhury, Influence of second-phase precipitates on the texture evolution of Mg–Al–Zn alloys during hot deformation, *Scripta Materialia* 66(3) (2012) 159-162.
- [26] E. Dogan, S. Wang, M.W. Vaughan, I. Karaman, Dynamic precipitation in Mg–3Al–1Zn alloy during different plastic deformation modes, *Acta Materialia* 116 (2016) 1-13.
- [27] L.L. Rokhlin, *Magnesium alloys containing rare earth metals: structure and properties*, 1st ed., CRC Press, London, 2003.
- [28] X. Gao, S.M. He, X.Q. Zeng, L.M. Peng, W.J. Ding, J.F. Nie, Microstructure evolution in a Mg–15Gd–0.5Zr (wt.%) alloy during isothermal aging at 250°C, *Materials Science and Engineering: A* 431(1) (2006) 322-327.
- [29] H. Zhou, W.Z. Xu, W.W. Jian, G.M. Cheng, X.L. Ma, W. Guo, S.N. Mathaudhu, Q.D. Wang, Y.T. Zhu, A new metastable precipitate phase in Mg–Gd–Y–Zr alloy, *Philosophical Magazine* 94(21) (2014) 2403-2409.
- [30] J.K. Zheng, R. Luo, X. Zeng, B. Chen, Nano-scale precipitation and phase growth in Mg–Gd binary alloy: An atomic-scale investigation using HAADF-STEM, *Materials & Design* 137 (2018) 316-324.
- [31] Y. Zhang, W. Rong, Y. Wu, L. Peng, J.-F. Nie, N. Birbilis, A detailed HAADF-STEM study of precipitate evolution in Mg–Gd alloy, *Journal of Alloys and Compounds* 777 (2019) 531-543.
- [32] N. Stanford, D. Atwell, M.R. Barnett, The effect of Gd on the recrystallisation, texture and deformation behaviour of magnesium-based alloys, *Acta Materialia* 58(20) (2010) 6773-6783.
- [33] W.X. Wu, L. Jin, F.H. Wang, J. Sun, Z.Y. Zhang, W.J. Ding, J. Dong, Microstructure and texture evolution during hot rolling and subsequent annealing of Mg–1Gd alloy, *Materials Science and Engineering: A* 582 (2013) 194-202.

- [34] H. Azzeddine, B. Mehdi, L. Hennet, D. Thiaudière, B. Alili, M. Kawasaki, D. Bradai, T.G. Langdon, An in situ synchrotron X-ray diffraction study of precipitation kinetics in a severely deformed Cu–Ni–Si alloy, *Materials Science and Engineering: A* 597 (2014) 288-294.
- [35] H. Azzeddine, A. Hanna, A. Dakhouche, T. Baudin, F. Brisset, Y. Huang, T.G. Langdon, Evaluation of Thermal Stability and Its Effect on the Corrosion Behaviour of Mg-RE Alloys Processed by High-Pressure Torsion, *Crystals* 13(4) (2023) 662.
- [36] Y.H. Zhao, X.Z. Liao, Y.T. Zhu, Z. Horita, T.G. Langdon, Influence of stacking fault energy on nanostructure formation under high pressure torsion, *Materials Science and Engineering: A* 410-411 (2005) 188-193.
- [37] N. Stanford, The effect of rare earth elements on the behaviour of magnesium-based alloys: Part 2 – recrystallisation and texture development, *Materials Science and Engineering: A* 565 (2013) 469-475.
- [38] S. Tighiouaret, A. Hanna, H. Azzeddine, L. Rabahi, A. Dakhouche, F. Brisset, A.-L. Helbert, T. Baudin, D. Bradai, On the evolution of microstructure, texture and corrosion behavior of a hot-rolled and annealed AZ31 alloy, *Materials Chemistry and Physics* 267 (2021) 124598.
- [39] H. Azzeddine, D. Bradai, T. Baudin, T.G. Langdon, Texture evolution in high-pressure torsion processing, *Progress in Materials Science* 125 (2022) 100886.
- [40] S. Sadi, A. Hanna, T. Baudin, F. Brisset, J.M. Cabrera, H. Azzeddine, Microstructure and texture evolution of ECAP-processed Mg-Ce alloy during isothermal annealing, *Materials Today Communications* 32 (2022) 103920.
- [41] J.J. Bhattacharyya, B. Radhakrishnan, G. Muralidharan, S.R. Agnew, Texture Evolution During Grain Growth of Magnesium Alloy AZ31B, in: M. Alderman, M.V. Manuel, N. Hort, N.R. Neelameggham (Eds.), *Magnesium Technology 2014*, Springer International Publishing, Cham, 2016, pp. 233-238.
- [42] D. Panda, R.K. Sabat, S. Suwas, V.D. Hiwarkar, S.K. Sahoo, Texture weakening in pure magnesium during grain growth, *Philosophical Magazine* 99(11) (2019) 1362-1385.
- [43] L.Y. Zhao, H. Yan, R.S. Chen, E.-H. Han, The preferential growth and related textural evolution during static recrystallization in a cold-rolled Mg–Zn–Gd alloy, *Journal of Magnesium and Alloys* 9(3) (2021) 818-828.
- [44] F. Guo, R. Pei, L. Jiang, D. Zhang, S. Korte-Kerzel, T. Al-Samman, The role of recrystallization and grain growth in optimizing the sheet texture of magnesium alloys with calcium addition during annealing, *Journal of Magnesium and Alloys* 8(1) (2020) 252-268.
- [45] X. Yang, Y. Okabe, H. Miura, T. Sakai, Annealing of a magnesium alloy AZ31 after interrupted cold deformation, *Materials & Design* (1980-2015) 36 (2012) 626-632.